ORIGINAL RESEARCH

Cell penetrating peptide-modified nanoparticles for tumor targeted imaging and synergistic effect of sonodynamic/HIFU therapy

Yizhen Li,[1–3,*] Lan Hao,[1,2,*]
Fengqiu Liu,[1,2] Lixue Yin,[3]
Sijing Yan,[4] Hongyun
Zhao,[1,2,5] Xiaoya Ding,[6]
Yuan Guo,[1,2] Yang Cao,[1,2]
Pan Li,[1,2] Zhigang Wang,[1,2]
Haitao Ran,[1,2] Yang Sun[1,2]

[1]Institute of Ultrasound Imaging & Department of Ultrasound, The Second Affiliated Hospital of Chongqing Medical University, 400010 Chongqing, People's Republic of China; [2]Chongqing Key Laboratory of Ultrasound Molecular Imaging, 400010 Chongqing, People's Republic of China; [3]Department of Cardiovascular Ultrasound and Non-invasive Cardiology, Sichuan Academy of Medical Science & Sichuan Provincial People's Hospital, Chengdu, Sichuan Province, 610072, People's Republic of China; [4]Chongqing Hospital of Traditional Chinese Medicine, Chongqing 400021, People's Republic of China; [5]Department of Gastroenterology, The Second Hospital Affiliated to Chongqing Medical University, Chongqing, 400010, People's Republic of China; [6]Department of Ultrasound, University-Town Hospital of Chongqing Medical University, Chongqing, 401331, People's Republic of China

*These authors contributed equally to this work

Correspondence: Haitao Ran; Yang Sun
Institute of Ultrasound Imaging & Department of Ultrasound, The Second Affiliated Hospital of Chongqing Medical University, 76 Linjiang Road, 400010 Chongqing, People's Republic of China
Tel +86 236 369 3180; +86 236 371 9612
Email ranhaitao@cqmu.edu.cn; 303507@hospital.cqmu.edu.cn

Background: Theranostics based on multifunctional nanoparticles (NPs) is a promising field that combines therapeutic and diagnostic functionalities into a single nanoparticle system. However, the major challenges that lie ahead are how to achieve accurate early diagnosis and how to develop efficient and noninvasive treatment. Sonodynamic therapy (SDT) utilizing ultrasound combined with a sonosensitizer represents a novel noninvasive modality for cancer therapy. Different ultrasound frequencies have been used for SDT, nevertheless, whether the effect of SDT can enhance synergistic HIFU ablation remains to be investigated.

Materials and methods: We prepared a nanosystem for codelivery of a sonosensitizer (methylene blue, MB) and a magnetic resonance contrast agent (gadodiamide, Gd-DTPA-BMA) based on hydrophilic biodegradable polymeric NPs composed of poly (lactic-co-glycolic acid) (PLGA). To enhance accumulation and penetration of the NPs at the tumor site, the surface of PLGA NPs was decorated with a tumor-homing and penetrating peptide-F3 and polyethylene glycol (PEG). The physicochemical, imaging and therapeutic properties of F3-PLGA@MB/Gd and drug safety were thoroughly evaluated both in vitro and in vivo. F3-PLGA@MB/Gd was evaluated by both photoacoustic and resonance imaging.

Results: F3-PLGA@MB/Gd NPs exhibited higher cellular association than non-targeted NPs and showed a more preferential enrichment at the tumor site. Furthermore, with good drug safety, the apoptosis triggered by ultrasound in the F3-PLGA@MB/Gd group was greater than that in the contrast group.

Conclusion: F3-PLGA@MB/Gd can work as a highly efficient theranostic agent, and the incorporation of targeted multimodal and combined therapy could be an encouraging strategy for cancer treatment.

Keywords: cell penetrating peptide, tumor targeted, image, sonodynamic, HIFU, nanoparticle

Introduction

Non-surgical and minimally invasive treatments such as radiofrequency therapy, microwave therapy and ultrasound-based therapy have been utilized to treat breast cancer as an alternative to surgical excision and are potentially beneficial to patients by reducing complications, improving cosmetic effects and reducing the hospital stay.[1] Therapeutic ultrasound is intrinsically featured for its high tissue-penetrating capability and avoidance of radioactive damage.[2] Therapeutic ultrasound can be divided into thermal and non-thermal ultrasound energy for treating diseases, which can be represented by high-intensity focused ultrasound (HIFU) and sonodynamic

therapy (SDT), respectively.[3,4] HIFU ablation, as a promising and non-invasive procedure for cancer therapy, has rapidly developed over the last decades in the treatment of solid tumors.[5] However, its disadvantages, such as lower therapeutic efficiency with increasing depths and reduced HIFU acoustic power with rapid blood flow, can often lead to the persistence of residual tumor cells because of incomplete HIFU ablation. Recently, combination therapy has become an important strategy for minimizing side effects and enhancing the therapeutic outcomes of cancer treatment.[6] Research on the combination of radiotherapy with HIFU and the characterization of HIFU for sono-chemistry applications have been carried out in some tumor treatment studies.[7–9]

SDT has gained much attention as a reactive oxygen species (ROS)-mediated cancer therapy and has achieved impressive anticancer effects in previous studies.[10–12] Possible mechanisms of SDT include pyrolysis, cavitation and generation of ROS (such as singlet oxygen and oxygen-containing radicals) or a combination of mechanisms.[4,13] However, it has been fully demonstrated that the generation of ROS from sonosensitizers by ultrasound irradiation plays the determining role in inducing cell death and promoting a favorable therapeutic outcome. As an ultrasound-based therapy, SDT has obvious advantages including intrinsically high tumor tissue penetration capability and the ability to precisely focus on tumor tissue, leading to accurate killing of tumor cells with minimal damage to adjacent normal tissue and breaking the depth barrier of photoactivation.[14] Nevertheless, there are some remaining problems that have hindered the widespread clinical application of SDT, such as its high cavitation threshold, its small therapeutic region and the low quantum yield of the sonosensitizer, which result in long treatment durations.[15] On the other hand, despite the most characteristic heat ablation mechanism of HIFU, there are some non-thermal ablation effects such as cavitation and mechanical effects, and as a result, toxic free radicals and singlet oxygen may also be generated during the HIFU process.[16]

Therefore, the efficient synergistic HIFU and SDT treatment is still a biggest challenge for these two non-invasive procedures. Methylene blue (MB) is a hydrophilic phe-nothiazine derivative, and a commercially available sonosensitizer.[17] MB is FDA approved for use in globine-mia, and it has received increasing attention for use in clinical applications, including diagnosis and histological staining.[18,19] Furthermore, MB can work as sonosensitizer for sonodynamic therapy,[20,21] as well as photoacoustic (PA)

imaging contrast agent,[22] which benefit to early diagnosis is another important aspect of theranostics. However, some drawbacks of MB have limited its further clinical applications for tumor treatment, such as inactivation in the biological environment through chemical changes to colorless MB and poor tumor localization.[23] On the other hand, advances in nanotechnology have provided a platform for cancer detection, treatment and monitoring. Therefore, we questioned whether the limitations of MB could be overcome by embedding it inside nanoparticles (NPs) to minimize its oxidation in the biologic environment and by attaching antibodies or tumor-specific peptides to the surface of the NPs for better absorption by tumor cells.[24]

Peptides play an important role in cancer therapy.[25] Many peptides exhibit potent anticancer activities and the mechanisms include inhibition of tumor angiogenesis, induction of tumor apoptosis, immunomodulatory function and etc.[26,27] F3 peptide is known for mediating dual-targeting delivery to specific tumor cells and tumor angiogenesis by selectively binding to nucleolin, which is expressed on the surface of tumor cells and tumor angiogenic endothelial cells. Moreover, F3 contains a CendR sequence that enables deep penetration of the tumor parenchyma and promotes local drug aggregation and absorption.[28] Among various nano/micro-biomaterials, poly (lactic-co-glycolic acid) (PLGA) is one of the most effective biodegradable polymeric NPs. Due to its controlled and sustained release properties, low toxicity, and biocompatibility with tissue and cells, it has been approved by the US FDA for use in drug delivery systems.[29]

In the present work, F3-targeted and multifunctional PLGA NPs to combine dual-modal imaging (PA and MRI imaging) and dual-modal therapy (sonodynamic therapy and HIFU ablation) were prepared. As mentioned above, photoacoustic imaging is a new promising hybrid imaging modality which combines advantages of optical imaging and ultrasound imaging, possess the characteristic of high spatial resolution and high penetration depth. Moreover, PA imaging augmented with molecular targeted contrast agents can enhance cancer imaging at the cellular and molecular levels.[30] Currently, magnetic resonance imaging (MRI) is considered to be the major imaging modality that can provide cellular and molecular information in cancer, although MRI suffers from limitations such as system complexity and low temporal resolution.[31] Therefore, we designed a nanoplatform that effectively coloads PA imaging (MB) and MRI contrast agents (Gd-DTPA-BMA) to integrate their individual strengths and optimize cancer molecular imaging

with high spatial resolution in real-time. MDA-MB-231 (triple negative) breast cancer cells and human umbilical vein endothelial cells (HUVECs) were used to evaluate the cellular association, biosafety and cytotoxicity of F3-PLGA@MB/Gd NP. Further studies were conducted in xenografts in nude mice to evaluate the tumor-targeting therapeutic efficiency and dual-imaging capability of the nanocarriers. Herein, we preliminarily focus on the short-term therapeutic effectiveness of the dual-modal therapy combining SDT and HIFU both in vitro and in vivo. Schematic illustration of microstructure of F3-PLGA@MB/Gd nanoparticle and procedure of this article are shown in Scheme 1.

Materials and methods
Preparation and characterization of MB-Gd-loaded and F3-targeted NPs
Synthesis of MAL-PEG-PLGA-F3
F3–Cys peptite (KDEPQRRSARLSAKPAPPKPEPKPKK APAKKC) was purchased from China Peptides Co., LTD. Heterobifunctional PEG (MAL–PEG–NHS, 3.5k) was supplied by Jenkem Technology Co., LTD. PLGA-(50:50, MW=10,000) was obtained from Daigang, China. MAL-PEG-PLGA-F3 was synthesized by Chongqing Protein Way Biotechnology Co., LTD.

Synthesis of Mb-Gd-loaded and F3-targeted NPs
F3-PLGA@MB/Gd was prepared as follows: First, 0.1 mL MB (5 mg/mL, 5 mg MB dissolved in 1 mL ddH2O, Sigma-Aldrich China) and 0.1 mL Gd-DTPA-BMA (287 mg/mL, GE Healthcare Ireland) were added to 3 mL CH_2CL_2 containing 50 mg dissolved MAL-PEG-PLGA-F3 and 6 mg dissolved MB. The sufficiently dissolved mixture was emulsified using an ultrasonic oscillator (SONICS &

MATERALS Inc., USA) at 100 W for 180 s. Subsequently, the above solution was decanted into 10 mL poly vinyl alcohol (PVA, MV=25 000, Sigma) solution (4% w/v) for the second emulsion by an ultrasonic oscillator at 50 W for 90 s. Next, the emulsion was stirred at room temperature for 2~5 h to extract CH_2CL_2. The supernatants were discarded after centrifugation at 10,000 rpm for 5 min, and the precipitate was suspended in 2 mL ddH2O. Centrifugation and generation of the suspension were performed three times.

Synthesis of fluorescence-labeled F3-PLGA@MB/Gd NPs
The preparation method of fluorescence-labeled NPs was similar to the procedure described above. Moderate DiI (Beyotime Institute of Biotechnology) or DiR (Beijing Fluorescence Biotechnology Co. Ltd.) fluorescent dyes were added to 3 mL CH_2CL_2. The other reagents were added as described above, and the mixture was emulsified twice, mixed and centrifuged.
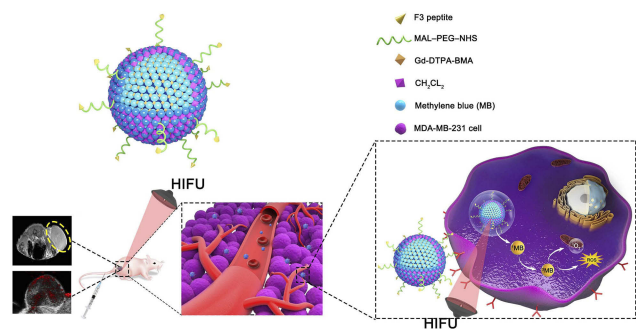
Characterization F3-PLGA@MB/Gd NPs
The morphology and structure of the NPs were evaluated by light microscopy (Olympus CKX41; CANADA), scanning electron microscopy (SEM, Hitachi S-3400N, Japan), and transmission electron microscopy (TEM, JEOL JSM-7800F, Japan), and a Malvern Zetasizer Nano ZS (Malvern Instruments, UK) system was used to measure their average diameter and electric potential. The fluorescence-labeled NPs were observed by confocal laser scanning microscopy (CLSM, Nikon Eclipse Ti laser scanning confocal microscope, Japan). The absorption spectrum of the NPs and the encapsulation efficiency of MB were analyzed by a Lambda 950 ultraviolet spectrophotometer (PerkinElmer Lambda 950, USA). The amount of Gd-DTPA-BMA was assessed by inductively coupled plasma-atomic emission spectroscopy (ICP-AES) (Thermo Scientific iCAP 6000 Series).

Scheme 1 Schematic illustration of microstructure of F3-PLGA@MB/Gd nanoparticle and combined application of HIFU and SDT for precise theranostics of breast cancer.
Abbreviations: PLGA, ploy(lactide-co-glycolic acid); HIFU, high intensity focus ultrasound; SDT, sonodynamic therapy.

Cell culture and establishment of animal model
MDA-MB-231 cells and HUVECs were purchased from the China Center for Type Culture Collection (Wuhan, China). Cells were cultured with RPMI-1640 medium containing 10% fetal bovine serum (FBS, Gibco, Australian origin) and 1% penicillin-streptomycin and incubated under a 5% CO_2 atmosphere at 37 °C.

BALB/c nude mice (4–6 weeks, female, weight=14–16 g) were purchased from Beijing HFK Bioscience Corporation and bred in the Experimental Animal Center of Chongqing Medical University under constant

temperature and humidity conditions. To establish the breast tumor model, MDA-MB-231 cells (1×10^6) in the logarithmic growth phase were harvested and suspended in 100 μL phosphate-buffered saline (PBS). The suspension was subcutaneously injected into the right flank of each nude mouse. All experimental protocols were approved by the Chongqing Medical University animal ethics committee and the national guidelines on the care and use of laboratory animals.

Biosafety of F3-PLGA@MB/Gd NPs in vitro

A Cell Counting Kit-8 (DOJINDO Chemical Technology Shanghai Co., Ltd) was used to detect the toxicity of the NPs in vitro. MDA-MB-231 cells at a density of 5×10^4 cells/mL were seeded into a 96-well plate. After 24 h of culture, the cells were divided into 7 groups, each group containing 5 wells. Next, 0.1, 0.2, 0.4, 0.6, 0.8, or 1.0 mg/mL NP suspension was added to the wells corresponding to each experimental group, while the medium in control wells was changed with fresh culture medium. After 12 h and 24 h, the cells were washed three times with PBS, and 100 μL 10% CCK8 solution was added to the wells. Then, the 96-well plates were analyzed spectrophotometrically at 450 nm with an EL X 800 UniversalMiemp plate reader (Bio-TEK instruments, Inc). Cytotoxicity was calculated by the following equation:

$$\text{Cytotoxicity }(\%) = [(As - Ab)] / [(Ac - Ab)]*100\%$$

where As represents the experiment group, Ab represents the background group, and Ac represents the control group.

Assessment of targeting efficiency in vitro
Assessment of targeting efficiency in vitro
MDA-MB-231 cells and HUVECs (1×10^5) were seeded in confocal dishes, and after 36 h, MDA-MB-231 cells were incubated with DiI-F3-targeted and DiI-non-targeted NPs (2 mg/mL) for 1 h, respectively. HUVECs were incubated with DiI-F3-targeted NPs. Then, the cells were fixed by 4% paraformaldehyde for 10 min. The nuclei were stained with DAPI (Beyotime Institute of Biotechnology, China) for 10 min, and the membrane were stained with DiO (Beyotime Institute of Biotechnology, China) for 3 min. To further detect the targeting efficiency of F3-NPs, MDA-MB-231 cells were observed by CLSM every 15 min

during the first hour of incubation with DiI-F3-PLGA@MB/Gd.

Assessment of the penetrating ability of 3D multicellular tumor spheroid (MCTS)
The hanging drop method was used for multicellular tumor spheroid fabrication.[32] MDA-MB-231 cells were harvested during the logarithmic growth phase, and 20 μL cells suspension at the densities of 1×10^5 was seeded under the lids of the cell culture plates; an adequate amount of PBS was added to the petri dishes. Ten days later, the tumor spheroids were formed and incubated with DiI-F3-targeted and DiI-non-targeted NPs (2 mg/mL) for 3 h in 24-well plates. Then, the fluorescent intensity was observed by CLSM, scanning 10-μm-thick layers.

Detection of ROS generation in vitro
The ROS generation in the solution was measured by using N, N-dimethyl-4-nitrosoaniline (RNO, Sigma-Aldrich, Co.) as an indicator. A solution containing PBS buffer (10 mL), RNO (6 mg), and histidine (1.5 g, Sigma-Aldrich, Co.) was prepared, and adjusted according to optical density (O.D) value of 0.8 at 440 nm, as assessed by a Lambda 950 ultraviolet spectrophotometer (PerkinElmer Lambda 950, USA). Then, 1 mL solution and 1 mL F3-PLGA@MB/Gd were mixed in the 24-well plates and treated with ultrasound gene transfection treatment meter (UGT) 1025 (Institute of Ultrasound Imaging of Chongqing Medical University, Chongqing, China) for 1 min, 2 min, 4 min, and 6 min at 1 MHz, 0.5 W/cm^2. The absorption values of the mixture at a wavelength of 440 nm were tested by a Lambda 950 ultraviolet spectrophotometer.

Intracellular ROS accumulation was detected by a DCF-DA fluorescent probe (Sigma-Aldrich, China). Briefly, MDA-MB-231 cells at a density of 10^5 cells/mL were seeded into laser confocal dishes and divided into the six following groups: I: Cells; II: Cells + ultrasound (US); III: PLGA+US; IV: MB+US; V: PLGA@MB/Gd +US; and VI: F3-PLGA@MB/Gd +US. After 3 h of incubation with PLGA, MB, PLGA@MB/Gd, or F3-PLGA@MB/Gd, the cells were washed three times with PBS, and groups II, III, IV, V, and VI were treated with ultrasound (1 MHZ, 0.5 w/cm^2, 30 s). Then, DCF-DA (0.4 mM/mL) was added to the dishes. Thirty minutes later, the dishes were observed by CLSM. Flow cytometry was used to further analyze the intracellular ROS levels among the six groups by DCF-DA. After 30 min incubation with DCF-DA, the

cells were washing and then resuspended in PBS and measured using a flow cytometer. A minimum of 10,000 cells per sample were acquired.

In vitro cytotoxicity assay of SDT

MDA-MB-231 were seeded into 96-well plates and divided into 6 groups. After 24 h, the MDA-MB-231 cells were incubated with PLGA, MB, PLGA@MB/Gd, or F3-PLGA@MB/Gd at a concentration of 1 mg/mL for 3 h. Next, after washing with PBS three times, 5 groups of cells were treated with ultrasound (1 MHZ, 0.5 w/cm^2, 30 s) on the bottom of the plates. Then, 10% CCK8 (100 μL) solution was added to the wells, and the OD values at 450 nm were tested by an EL X 800 UniversalMiemp plate reader.

Apoptotic cells were counted by flow cytometry (FCM). MDA-MB-231 cells were seeded into six-well plates. After incubation and ultrasound treatment, the cells of 6 groups were harvested using 0.25% trypsin-EDTA (Beyotime Institute of Biotechnology, China), centrifuged at 1000 r/5 min and suspended in 1 mL PBS for FCM.

PA and MRI dual-modality imaging in vitro

For PA imaging in vitro, 100 μL F3-PLGA@MB/Gd NP solution at various concentrations (5 mg/mL, 7.5 mg/mL, 10 mg/mL, 15 mg/mL, 20 mg/mL, 25 mg/mL) were placed into a gel module (prepared with a 200 μL pipette tip box), and the PA intensity variation was detected at a wavelength of 700 nm by using a Vevo LAZR photoacoustic imaging system (VisualSonics Company, Canada).

For MRI imaging in vitro, 2 mL NP aqueous solutions with various dilution ratios were added to 4 mL centrifuge tubes. All the tubes were fixed and then evaluated by MR imaging using a Philips Achieva 3.0T magnetic resonance scanner (Royal Dutch Philips Electronics Ltd.). Experimental parameters: Act. TR/TE (ms): 190/2.2, min TR/TE (ms): 53/2.2, scan percentage: 80.9%, NSA: 4.

Biosafety of F3-PLGA@MB/Gd NPs in vivo

Serum biochemical parameters were analyzed to evaluate the biosafety in vivo. Kunming mice (n=15, 4–6 w, female, weight=15–20 g) were divided into three groups, and the F3-PLGA@MB/Gd NP solution (10 mg/mL) was injected intravenously. After 7, 15, and 30 days, the whole blood of mice was sampled by enucleating their eyeballs and centrifuged at 3000 rpm for 10 min. The serum was collected to detect liver (ALT, AST), cardiac (CK, LDL-C) and kidney (UA, Cn, BUN) function.

Assessment of targeting efficiency in vivo

The nude mice bearing MDA-MB-231 tumors were divided into two groups (n=10). After peritoneal injection of 1% pentobarbital sodium, 200 μL DiR-F3-PLGA@MB/Gd and DiR-PLGA@MB/Gd NPs (10 mg/mL) were injected intravenously. The fluorescent distribution was detected by IVIS Spectrum (Caliper Life Science, Hopkinton, MA, USA). Images were taken at predetermined time points (1 h, 2 h, 4 h, 6 h, 12 h, 24 h). After 24 h, the mice were sacrificed, and organs were imaged.

DiI-F3-PLGA@MB/Gd and DiI-PLGA@MB/Gd (10 mg/mL) were used to further validate the targeting efficiency in vivo. Frozen tissues were cryosectioned, fixed with 4% paraformaldehyde and stained with DAPI. Anti-fade reagent was added, and finally, histological sections were assessed by CLSM.

PA and MRI dual-modality imaging in vivo

When the tumor sizes reached 8–10 mm, fifteen tumor-bearing mice were anesthetized and underwent PA and MRI dual-modality imaging. After intravenous injection with saline, targeted and non-targeted NP solutions (0.2 mL, 10 mg/mL), the tumors were imaged at set time points (1 h, 2 h, 4 h, 6 h, 12 h, 24 h). The experimental parameters were as follows: Vevo LAZR photoacoustic imaging system: wavelength:700nm; PA gain:50dB; depth: ≤11 mm. Philips Achieva 3.0T magnetic resonance scanner: Act. TR/TE (ms): 0/2.2, min TR/TE (ms): 53/2.2, scan. percentage: 80.9%, NSA: 4.

HIFU exposure in vitro and in vivo

A JC200 HIFU ablation device (Chongqing Haifu Technology Center, Chongqing, China) was applied for the experiment. HIFU exposure in vitro was performed with fresh bovine liver tissue (10 cm*10 cm*8 cm). The tissue samples were placed in a container and immersed in degassed water for 30 min. After the degassing process, the specimens were injected with 200 μL solution and divided into five groups—HIFU group, HIFU+PBS group, HIFU+PLGA group (10 mg/mL), HIFU+MB group, and HIFU+ PLGA@MB/Gd group—each with the same MB concentration (1.3 mg/mL). HIFU ablation was performed on the injection site via single irradiation with output acoustic powers of 120 W for 3 s.

For the in vivo study, 30 tumor-bearing mice were divided into six groups (n=5): group I (HIFU), group II (HIFU+PBS), group III (HIFU+PLGA), group IV (HIFU+MB), group V (HIFU+ PLGA@MB/Gd), and group VI

(HIFU+ F3-PLGA@MB/Gd). In groups II~VI, the agent was injected via the tail vein (200 μL, 10 mg/mL), six hours later the nude mice were anesthetized and placed in the lateral decubitus position on the HIFU treatment bed. The following experimental parameters were used according to the previous study: 120 W, 3 s, one single exposure.

During the experiment, the gray scale of the tumor site pre- and post-ablation were recorded by Gray Val 1.0 software (Chongqing Haifu Medical Technology Co., Ltd., China). Diagnostic ultrasound images in real time were used to evaluate ablation effects. Coagulated necrosis volumes were calculated by HIFUJupiter 1.0 software (Chongqing Haifu Medical Technology Co., Ltd., China

After HIFU ablation, the mice were euthanized, and the tumors were immediately removed and fixed with 4% paraformaldehyde. Hematoxylin and eosin (HE) stain was used for the histopathological assay. For immunohistochemical examination, proliferating cell nuclear antigen (PCNA) and TdT-mediated dUTP nick end labeling (TUNEL) were used to evaluate proliferation and apoptosis in the targeted tissues. The proliferative index (PI) and the apoptotic index (AI) were calculated as the ratio of positive cells from 5 random fields at 400× magnification.

Statistical analysis

Data were presented as the means ± the standard deviations (SD). Statistical analysis was performed with GraphPad Prism version.5.01(GraphPad Software, Inc., CA, USA) through Student's t-test and One-way ANOVA. Statistical significance was set to $P<0.05$.

Results and discussion
Characterization of F3-NPs

MAL-PEG-PLGA-F3 was successfully synthesized and purified, the analysis of proton nuclear magnetic resonance spectra (NMR) and HPLC verified that F3 peptide and PEG were successfully connected to PLGA (Figure S1 and Figure1A and B). Figure 1C–E show optical microscopy, SEM and TEM images of F3-PLGA@MB/Gd NPs. Figure 1F shows a CLSM image of DiI-F3-PLGA@MB/NPs. As these representative images demonstrated, the NPs were blue and had a smooth, uniform spherical morphology, with MB covering the shells and MB/Gd-DTPA-BMA within the cores. The NPs could be stained by DiI and exhibited red fluorescence detected with CLSM. The mean diameter of the F3-NPs was 242.6±71.15 nm (PDI=0.218), and the zeta potential was −18.4±3.41 mV (Figure 1G and H).

The ultraviolet (UV) absorption spectra of MB and F3-NPs are shown in Figure S2, both with the highest peak at approximately at 670 nm, which indicated that MB was efficiently added to the NPs. The encapsulation efficiency and the drug-loading efficiency were 41.53 ±3.30% and 3.22±0.255%, respectively, for MB and were 29±9.46% and 2.44±0.796% for Gd-DTPA-BMA according to the ICP detection.

For the drug delivery system (DDS), the nanocarrier size and surface modifications (pegylation and surface charge) are necessary prerequisites and significant factors in determining blood residence time and organ-specific accumulation.[33] The average diameter of F3-NPs was 242.6 nm, indicating that most of the F3-NPs were in the reported particle size range (cutoff size of >400 nm) for the enhanced permeability and retention (EPR) effect and for targeted imaging and therapy.[34]

To achieve good PA images and to increase ROS production, we used supersaturated liquid of MB both in CH_2CL_2 and ddH_2O. In fact, we tested three methods of NP preparation: encapsulation in the core, coating on the surface, and both encapsulation in the core and coating on the surface. We found that the third method led to the best PA imaging. In addition, these characterizations indicated that the supersaturated MB liquid and the F3 peptide on the surface cause no visible differences in the UV absorption characterization or in the spherical appearance and nanoscale particle size.

Assessment of targeting efficiency in vitro

Nucleolin, which is expressed only in normal cell nuclei but is overexpressed on the surface of tumor cells and tumor angiogenic endothelial cells, has become a molecular target for the specific delivery with nanotechnology-based therapy.[35] Moreover, according to the previous study from Nuno A. Fonseca et al, nucleolin was a common receptor among breast cancer cells.[36] Herein, the cellular analysis of the tumor-homing and penetration efficiency of F3-NPs was carried out with MDA-MB-231 breast cancer cells and HUVECs. As shown in Figure 2A and B, among the three groups, MDA-MB-231 cells incubated with F3-NPs displayed the strongest fluorescence, while HUVECs exposed to F3-NPs and MB-231 cells exposed to non-targeted NPs exhibited non-obvious fluorescence changes. HUVECs are normal cells which nucleolin is mainly expressed in the nuclei, and thus could explain the reason why nanoparticles did not targeted HUVECs. To further investigate the disassembly process of F3-NPs
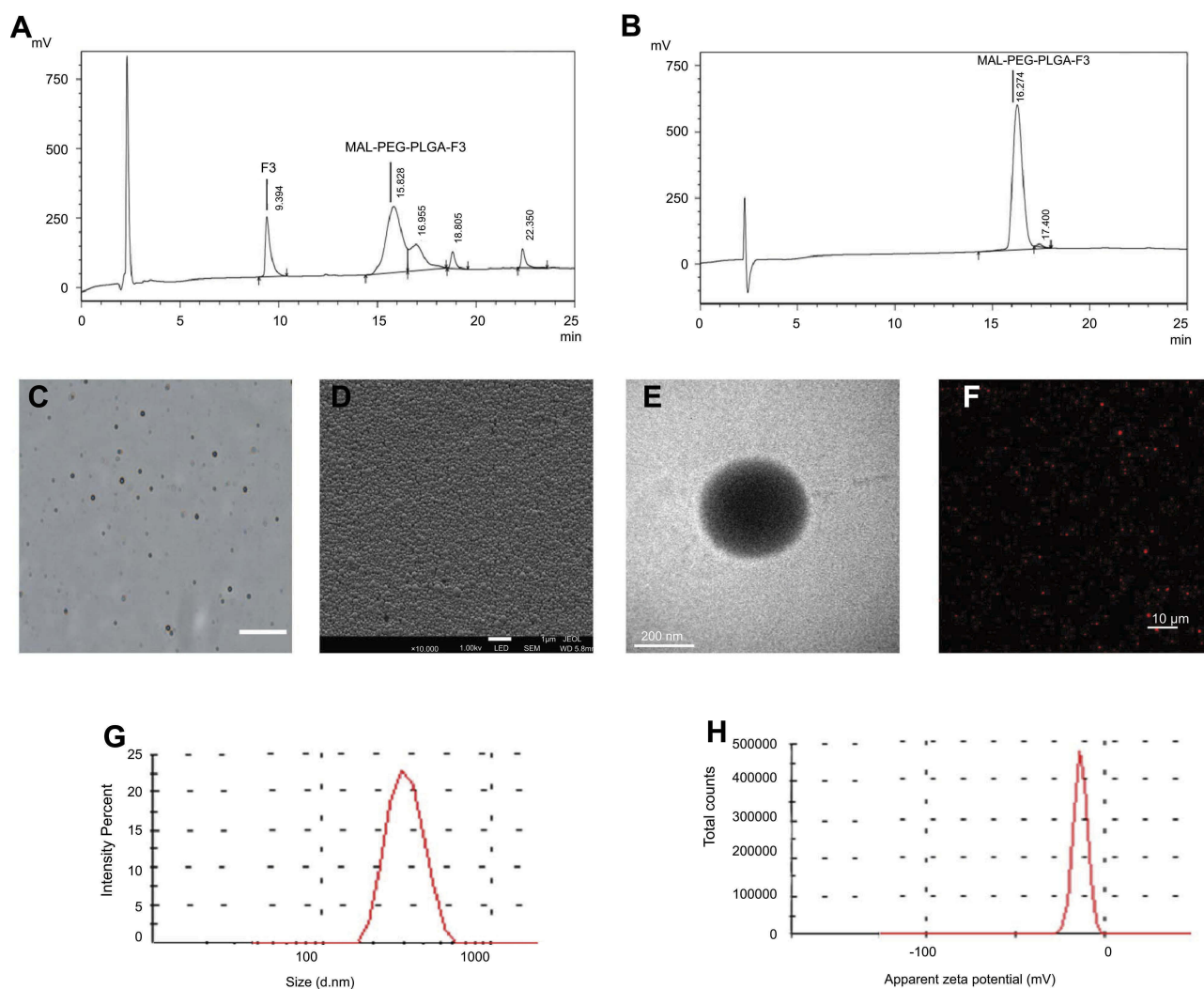
Figure I (**A**) HPLC analysis of MAL-PEG-PLGA-F3 after modification. (**B**) HPLC analysis of MAL-PEG-PLGA-F3 after purification. (**C**) Optical microscopy image of F3-PLGA@MB/Gd NPs, scale bar: 20 μm. (**D**) SEM image of F3-PLGA@MB/Gd NPs, scale bar: 1 μm. (**E**) TEM image of F3-PLGA@MB/Gd NPs, scale bar:200 nm. (**F**) CLSM image of Dil-F3-PLGA@MB/Gd NPs, scale bar: 10 μm. (**G**) Size distribution of F3-PLGA@MB/Gd NPs. (**H**) Zeta potential of F3-PLGA@MB/Gd NPs (n=3).
Abbreviations: HPLC, high performance liquid chromatography; MAL, maleimide; PEG, polyethylene glycol; PLGA, poly(lactide-co-glycolic acid); NPs, nanoparticles; SEM, scanning electron microscope; TEM, transmission electron microscope; CLSM, confocal laser scanning microscope.

in MB-231 cells, the incubation procedure was observed over 1 h by CLSM. The result (Figure S3) showed that DiI fluorescence could be detected quickly after 5 min incubation, and the intensity was gradually enhanced with time, which indicated the efficient targeting ability of F3-NPs.

3D multicellular tumor spheroid (3D MCTS) was used to simulate internal solid tumor tissue. Due to the viable rim, gradients of oxygen tension, nutrients, catabolites, and cell proliferation are identical to the internal tumor microenvironment. Therefore, these spheroids possess several advantages over monolayer tumor cells.[37] Here, we used 3D MCTS to study the F3 peptide-mediated penetration efficiency. Figure 2C and

D showed laser confocal images for 3D MCTS, the non-targeted group displayed weak fluorescent intensity, while the F3-NPs group demonstrated remarkably higher fluorescence intensity throughout the tumor spheroids. Quantitative analysis of 3D-MCTS from bottom to top layers presented that the fluorescence intensity value in F3-targeted group was 2.58-fold higher than that of non-targeted group at the top layer, and 8.15-fold higher than that at the bottom layer (Figure 2E). This finding indicates that F3-decorated NPs could be recognized and taken into the inner region of solid tumors, which is considered a cornerstone to cancer therapy.
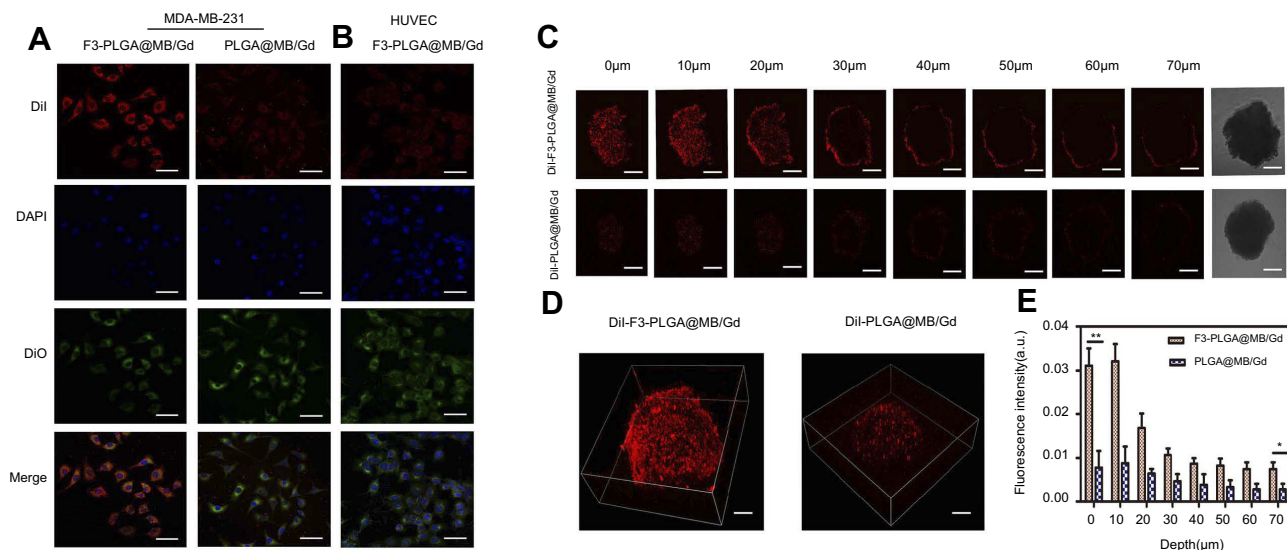
Figure 2 (**A**) CLSM images of MDA-MB-231 cells incubated with Dil-labeled F3-targeted NPs and non-targeted NPs. From top to bottom are Dil-labeled nanoparticles, the DAPI-labeled nuclei, DIO -labeled cytolemma and their overlay, scale bar: 50 μm. (**B**) CLSM images of HUVEC cells incubated with Dil-labeled F3-targeted NPs. (**C**) Multi-level scan at 10 μm intervals for the penetration of Dil-F3-PLGA@MB/Gd NPs and Dil-PLGA@MB/Gd NPs(left) and confocal images of MDA-MB-231 tumor spheroids (right). Scale bar: 250 μm. (**D**) 3D-reconstruction of the MDA-MB-231 tumor spheroids in the Dil-F3-PLGA@MB/Gd group and Dil-PLGA@MB/Gd group. (**E**) Quantitative analysis of fluorescence intensity value in F3-targeted group and non-targeted group (*$P<0.05$, **$P<0.01$).
Abbreviations: CLSM, confocal laser scanning microscope; NPs, nanoparticles; HUVEC, human umbilical vein endothelial cells; PLGA, poly(lactide-co-glycolic acid); MB, Methylene blue; Gd, gadodiamide;3D, three-dimensional.

## Detection of ROS generation in vitro

Thus far, it has been fully demonstrated that the generation of ROS from sonosensitizers by ultrasound irradiation plays the determining role in inducing cell death and contributing to therapeutic outcomes. To reveal the ROS generation capacity of the F3-PLGA@MB/Gd NPs, suspensions of these NPs in PBS (PH 7.4) containing RNO and histidine were incubated and treated with US (0.5 w/cm^2) for various amounts of time. The underlying mechanism is that RNO is oxidized by the intermediate product derived from the reaction between histidine and ROS, leading to decreased RNO absorbance at 440 nm ("RNO decolorizing reaction").[38] As expected, the absorption values at 440 nm of RNO incubated with the F3-PLGA@MB/Gd NPs decreased with increasing US exposure time, which indicated that RNO could generate ROS upon triggering by US and, thus, has the ability to kill tumor cells in SDT. (Figure S4)

Intracellular ROS levels under US wave irradiation were investigated by using DCF-DA as the ROS staining indicator (Figure 3A and B). The PLGA@MB/Gd +US group exhibited stronger fluorescence than the free MB +US group, suggesting that NPs could protect the sono-character of MB and, thus, could enhance the efficiency of ROS generation. Furthermore, the F3-PLGA@MB/Gd +US group exhibited the strongest green fluorescence

compared with the other five groups, indicating that engineering the surface of NPs with F3 peptide could facilitate the accumulation of NPs in tumor cells and lead to an increased ROS yield upon triggering by US. Figure 3C shows that the fluorescence spectral curve shifted more significantly to the right in F3-PLGA@MB/Gd NPs mediated SDT group than other groups. This demonstrates that F3-PLGA@MB/Gd NPs mediated SDT remarkably increased the intracellular ROS level.

Cytotoxicity assay of SDT in vitro

The outstanding ROS generation of F3-PLGA@MB/Gd prompted us to investigate the therapeutic efficacy of the NPs in more detail. Before evaluating the sonodynamic effect of F3-PLGA@MB/Gd in vitro, we measured the biosafety of the NPs with MDA-MB-231 triple-negative breast cancer cells (Figure S5). The result showed that the cell viability was approximately 90% at all time points, and the values exhibited no significant difference from the 0.1 to 1 mg/mL groups, indicating that F3-PLGA@MB/Gd is cytocompatible. In addition, biosafety in vivo was evaluated in Kunming mice by assessing various serum biochemical parameters. As shown in Figure S6, ALT, AST, CK, LDL-C, UA, Cn, and BUN values were steady throughout the 30-day test, suggesting that F3-PLGA@MB/Gd NPs exhibited good biocompatibility.
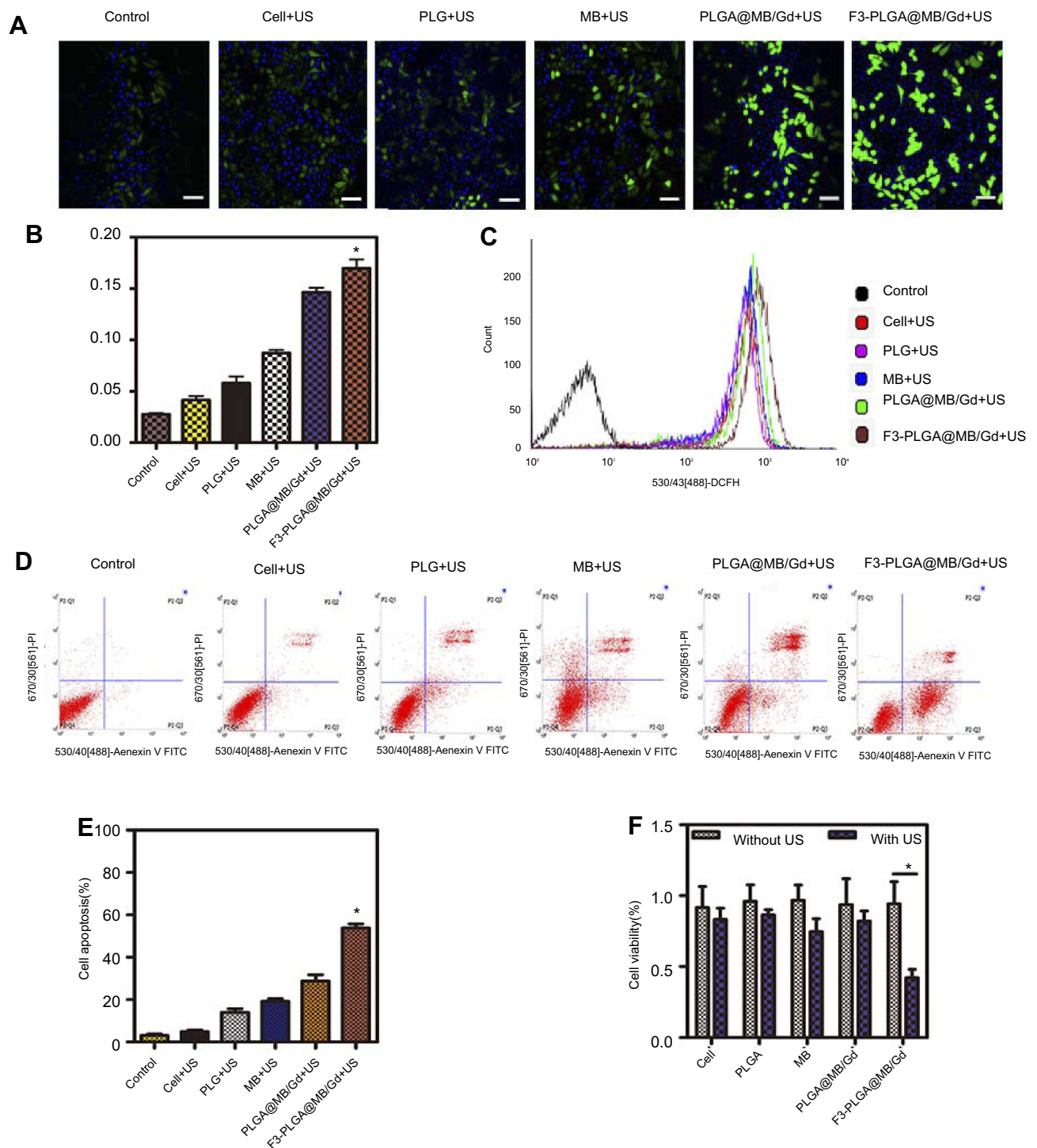
Figure 3 (**A**) CLSM images of intracellular ROS under US wave irradiation (0.5W, 30s) in various groups. Scale bar: 50 μm. (**B**) Quantitative analysis of CLSM images (*$P<0.05$). (**C**) Measurement of ROS in MDA-MB-231 cells of various groups with DCFH-DA staining by using flow cytometry under the US irradiation (0.5 W, 30s). (**D**) Apoptosis detection by flow cytometry in various groups. (**E**) Quantitative analysis of apoptosis as determined by FCM (*$P<0.05$). (**F**) Cell viabilities as measured by the CCK-8 assay (*$P<0.05$).
Abbreviations: CLSM, confocal laser scanning microscope; ROS, reactive oxygen species; US, ultrasound; FCM, flow cytometry.

FCM was utilized to quantitatively assess the extent of apoptosis induced by the NPs on MB-231 cells during the sono-activated treatment (Figure 3D and E). The result showed that the F3-PLGA@MB/Gd NPs combined with US corresponded to significantly increased early and late apoptotic and necrotic cell populations (53.86±3.34)%, while the non-

targeted NPs +US, MB +US, PLGA +US, Cell + US and Control groups corresponded to apoptotic and necrotic cell populations of (28.76±5.06)%, (19.20±5.13)%, (14.08 ±3.39)%, (4.96±1.33)% and (3.09±1.24)% respectively.

Ultrasound sensitivity was also validated by CCK8 assay in MDA-MB-231 cells (Figure 3F). Cells were divided into various experiment groups (with US) and corresponding contrast groups (without US). There was no obvious cell death in the contrast groups, while all the experimental groups exhibited different degrees of decreased cell viability, and the F3-NPs group showed the lowest cell survival rate ($P<0.05$).

Earlier studies have suggested that micro/NPs can enhance SDT efficiency based on several considerations.[39,40] According to our present study, four main factors could be involved: First, nanosized PLGA particles can improve the capability of intracellular delivery. Second, surface modification of F3-targeted peptides, which are characterized by deep penetration and tumor-homing abilities, can facilitate the accumulation of the sonosensitizer in deep-seated tumors. Third, the preservation and sustained release of MB from PLGA NPs can retain the sonochemical property of MB. Moreover, PLGA NPs can act as energy transducers to further enhance the efficiency of SDT.

Assessment of targeting efficiency in vivo

In addition, to determine the bio-distribution and tumor-targeting efficiency of the NPs, an in vivo imaging system (IVIS) was used. At all the time points, the tumor site fluorescence intensity in the F3-targeted group was higher than that in the non-targeted group. In the F3-targeted group, the fluorescence continued to increase, followed by accumulation and steady fluorescence at 6 h, thereafter moderate clearance was observed. In contrast, the fluorescence intensity in the non-targeted group underwent a rapid and consistent clearance process within 24 h (Figure 4A). The fluorescence intensity ratio was calculated by the tumor to background ratio (TBR).[41] The TBRs at different post-injection time intervals in the targeted group were much higher than those in the non-targeted group ($P<0.05$) (Figure 4C). This result was confirmed by the fluorescence intensity in tumor and main organs at 24 h post-injection in both groups (Figure 4B and D). The fluorescence of the tumor region in the F3-targeted group was 2-fold stronger than that in the non-targeted group ($P<0.05$).

Frozen tissues slices were prepared, and images were captured by CLSM (Figure 4E). Consistently, tumor ultra-thin sections at 24 h post-injection revealed that the red

fluorescence intensity of the tumors was much stronger in the DiI-F3-NPs group than in the non-targeted group, although the fluorescence of the liver was equal in both groups. Thus, this result was concordant with the in vivo imaging and could be explained by the continuous accumulation induced by active targeting and the EPR effect of F3-targeted NPs at the tumor site, while non-targeted NPs were metabolized immediately. Thus, the F3-targeted NPs led to increased specificity and efficacy against breast tumors relative to their non-targeted counterparts.

PA and MRI dual-modality imaging in vitro and in vivo

PA/MRI dual-modality imaging properties of the F3-NPs in vitro were evaluated. The F3-NPs demonstrated a linear signal dependency of the T1 intensity values (Figure 5A), Figure 5B showed that the PA signal intensity increased with various concentrations using 710nm for excitation, and the maximum concentration showed the strongest PA signal. Additionally, the PA/MRI dual-modality imaging properties of F3-NPs in vivo were assessed by comparing to two controls: non-targeted NPs and saline. As showed in Figure 5C and E, these dynamic images further showed that high-resolution PA and MRI imaging of the tumor site could be performed in the F3-PLGA@MB/Gd NPs group and that the tumor signals were primarily concentrated at 6 h post-injection. In contrast, both the PA and MRI signals in the non-targeted group were much lower, and no obvious concentration could be observed in the tumor region. The saline group exhibit no signals on bi-modality imaging. Quantitative analysis results (Figure 5D and F) also demonstrated this phenomenon.

As seen, F3-PLGA@MB/Gd showed great potential for use as both a PA imaging contrast agent and a MRI contrast agent. This property could aid in image-guided therapies and in detecting the functional characteristics of tumors.

HIFU exposure in vitro and in vivo/ histopathological and immunohistochemistry detection

Many previous studies have considered HIFU synergy as a way to overcome incomplete tumor ablation. However, the combination of SDT and HIFU therapy could also be an efficient method to solve this problem. Herein, we introduced PLGA@MB/Gd to HIFU irritation in vitro. A relatively small acoustic power of 120 W and a short exposure time of 3 s were selected according to previous studies.[42]
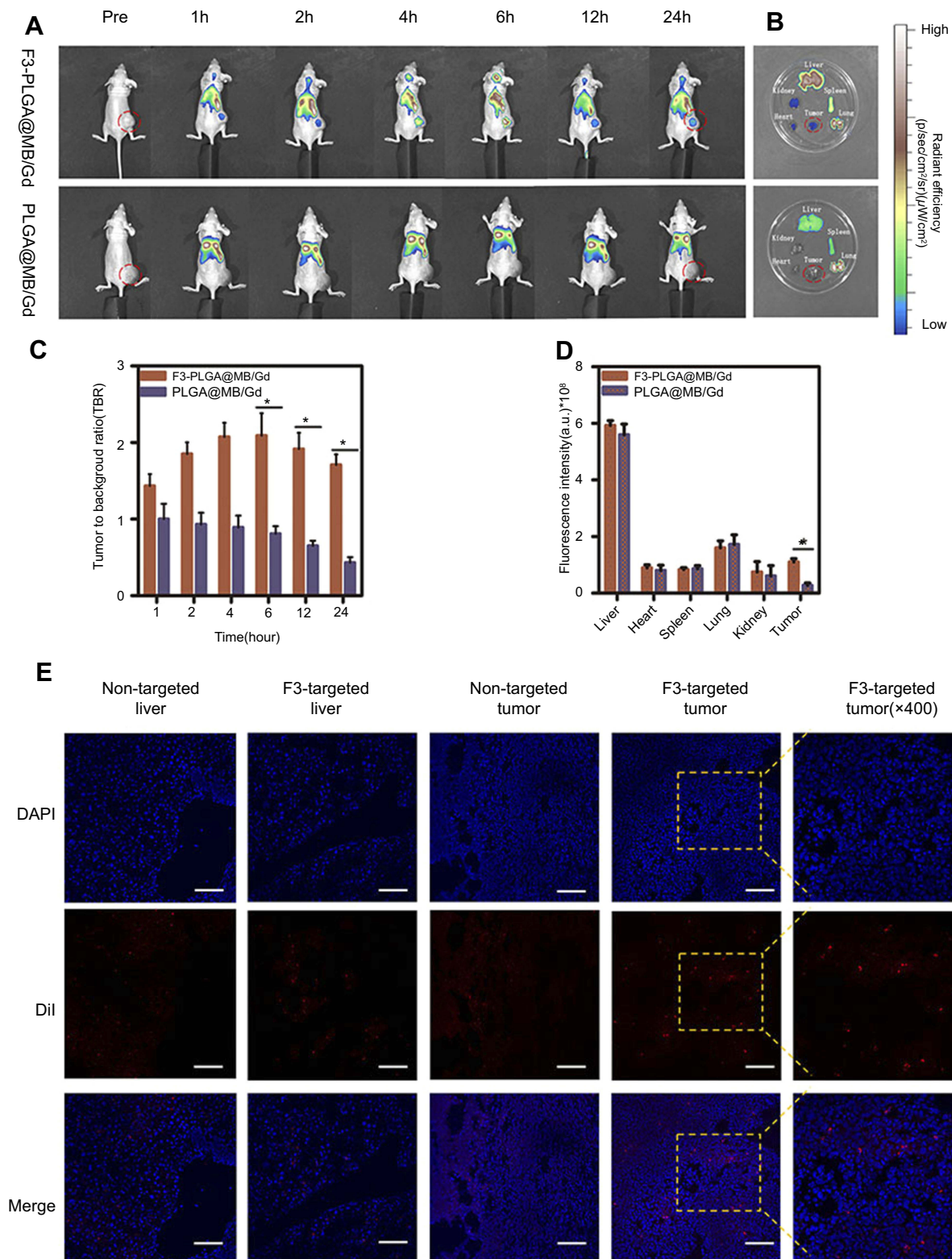
Figure 4 (**A**) In vivo imaging system (IVIS) fluorescence images of the nude mice bearing MDA-MB-231 tumors 1h, 2h, 4h, 6h, 12h, 24h after intravenous administration of DiR-labeled F3-PLGA@MB/Gd NPs and DiR-labeled PLGA@MB/Gd NPs. (**B**) Ex vivo fluorescence imaging of tumor and main organs 24h after intravenous administration of DiR-labeled F3-PLGA@MB/Gd NPs and DiR-labeled PLGA@MB/Gd NPs. (**C**) In vivo tumor-to-background ratios after different time points intravenous injection. (**D**) Quantification of fluorescence intensity of tumor and dissected organs. (**E**) DiI-labeled F3-PLGA@MB/Gd NPs or PLGA@MB/Gd NPs distribution in tumor and liver tissues. Scale bar: 50 μm. *P<0.05.

**Abbreviations:** NPs, nanoparticles; PLGA, poly(lactide-co-glycolic acid); MB, Methylene blue; Gd, gadodiamide.
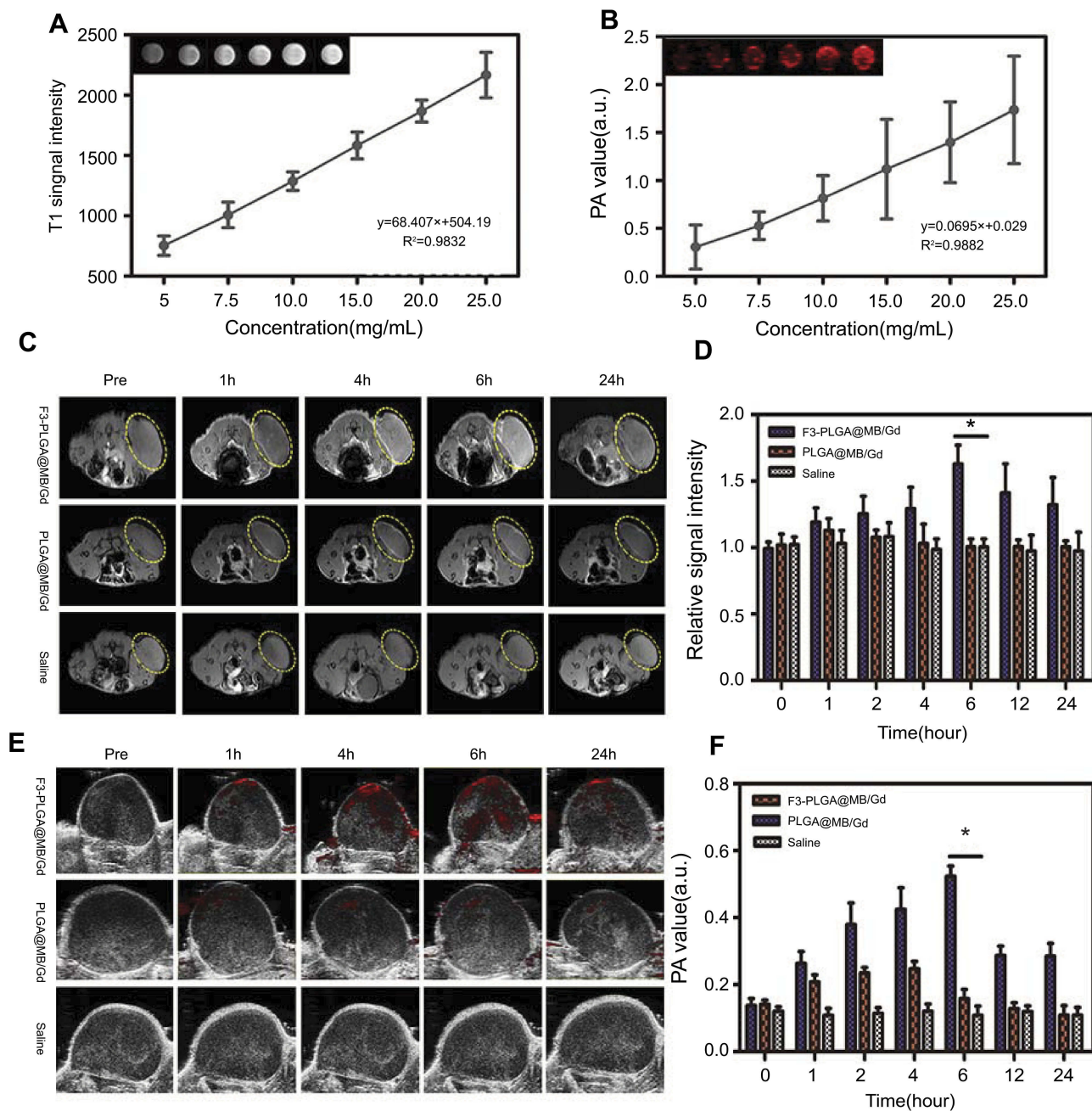
Figure 5 (**A**)In vitro T1W1 MR images and MRI signal intensities of F3-PLGA@MB/Gd NPs solution at different concentrations (5.0, 10, 15, 20, 25 mg/mL). (**B**) In vitro PA images and PA values of F3-PLGA@MB/Gd NPs solution at different concentrations (5.0, 10, 15, 20, 25 mg/mL). (**C**) In vivo T1W1 MR images and the corresponding MRI signal intensities (**D**) post injection of F3-PLGA@MB/Gd NPs, PLGA@MB/Gd NPs, and saline at different time points (n=3 per group, *$P<0.05$). (**E**) In vivo PA images and corresponding PA values (**F**) Post injection of F3-PLGA@MB/Gd NPs, PLGA@MB/Gd NPs, and saline at different time points (n=3 per group, *$P<0.05$).
Abbreviations: MRI, magnetic resonance imaging; PLGA, poly(lactide-co-glycolic acid); MB, methylene blue; Gd, gadodiamide; NPs, nanoparticles; PA, photoacoustic.

The result (Figure 6A and B) showed that the gray scale variation value and the degree of coagulated necrosis in PLGA@MB/Gd + HIFU group experienced a greater change than the other groups. As shown in Figure 6D and E, the quantitative coagulation necrosis volume in PLGA@MB/Gd + HIFU group (63.91±6.42 mm^3) was nearly 9 times larger than the HIFU group (7.53 ±1.86 mm^3), while the necrotic volume in PLGA@MB/ Gd + HIFU group was 3 times larger than the PLGA +HIFU group (21.73±6.86 mm^3), and 2 times larger than the MB+HIFU group (30.72±6.86 mm^3). This indicates that PLGA@MB/Gd NPs has the potential to be used as synergistic ablative agent in HIFU therapy. Furthermore, MB embedded in PLGA was supposed to prevent MB
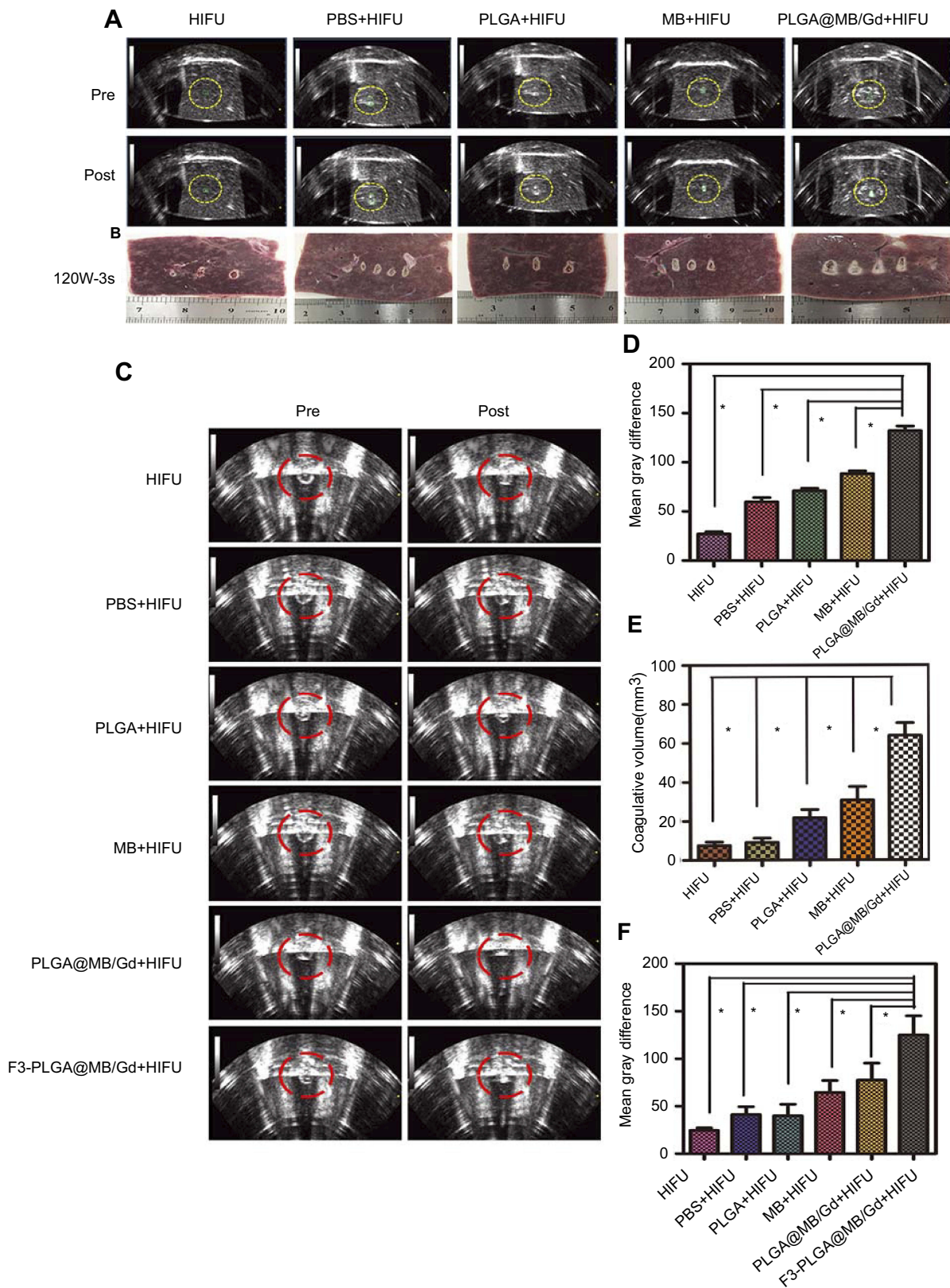
Figure 6 (**A**) B-mode ultrasound images of degassed bovine livers before and after HIFU exposure at 120 w, 3 s. (**B**) Digital photos of degassed bovine livers under HIFU irradiation after intra-tissue injection of various agents: PBS, PLGA, MB, PLGA@MB/Gd. (**C**) B-mode ultrasound images of MDA-MB-231 tumor tissues before and after HIFU exposure at 120 w, 3 s. (**D**) The mean grey difference calculation based on the ultrasound imaging of bovine liver tissue after various treatment. (*P<0.05). (**E**) The calculated coagulation volume of bovine liver tissue after HIFU treatments (*P<0.05). (**F**) The mean grey difference calculation based on the ultrasound imaging of MB-231 tumor tissue after HIFU treatment (*P<0.05).
Abbreviations: B-mode, brightness-mode; HIFU, high intensity focus ultrasound; PBS, phosphate buffer saline; PLGA, poly(lactide-co-glycolic acid); MB, methylene blue; Gd, gadodiamide.
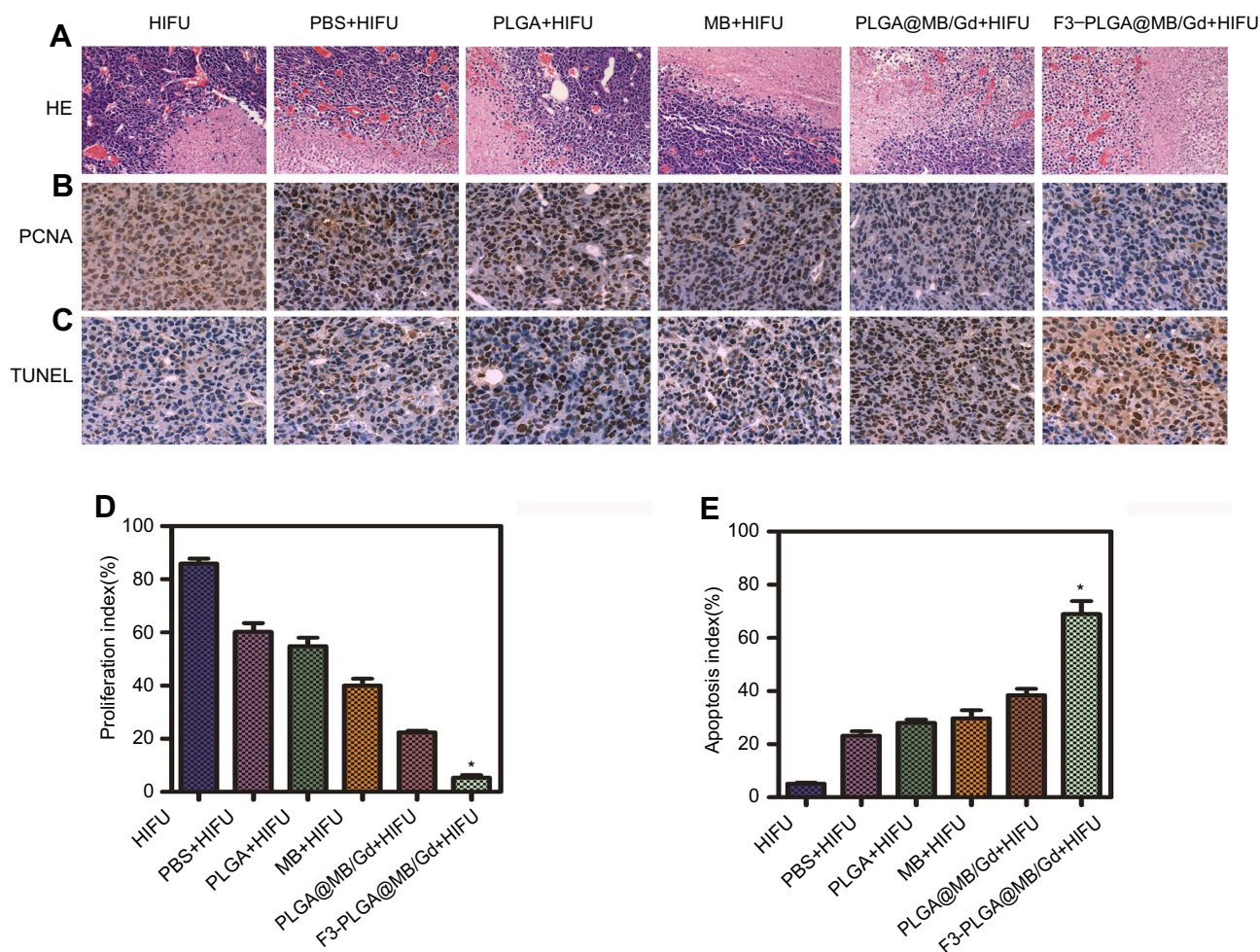
Figure 7 (**A**) H&E staining (magnification, 100×), (**B**) PCNA staining (magnification, 400×) and (**C**) TUNEL staining (magnification, 400×) of MDA-MB-231 tumor tissues in various groups after HIFU ablation. (**D**) proliferative index and (**E**) apoptosis index in various groups. (*$P<0.05$).
Abbreviations: H&E, hematoxylin-eosin; PCNA, proliferating cell nuclear antigen; TUNEL, terminal deoxynucleotidyl transferase-mediated dUTP nick end labeling.

from oxidation and keep sonodynamic activities. The coagulation necrosis in MB group could be enhanced after encapsulated in PLGA, which suggests that the sonodynamic activities of MB may play a role in synergistic ablative to some extent.

The anti-tumoral effect of HIFU combined with F3-PLGA@MB/Gd NPs was systematically detected with xenograft tumors in the nude mouse model. After HIFU irritation, the acoustic signal of tumor tissues (Figure 6C and F) varied significantly in different groups, where the mean gray scale difference in the F3-PLGA@MB/Gd NPs group was significantly higher than that in the PBS control group and the non-targeted group ($P<0.05$). To investigate the cell damage soon after HIFU irradiation treatment, tumors were removed 1 h later and fixed for histological and immunohistochemical detection. On microscopic examination, groups I to VI exhibited various extents of

coagulative necrosis after HE staining. The large-scale tumor necrosis were observed in group V and group VI, nuclear fragmentation and lysed cell membranes could be observed in the coagulation necrotic tissue and its surroundings, while the tumor cells around the coagulation necrotic tissue were observed to be arranged in nests in the HIFU group, the PBS+HIFU group and the PLGA+ HIFU group. (Figure 7A)

PCNA and TUNEL immunohistochemical staining was used to detect cell proliferation and apoptosis, respectively, and positive expression was demonstrated as brown nuclear staining. The results showed that, after HIFU irritation, the expression of PCNA was reduced or nearly absent in group VI and noticeable in group I, with a decreasing trend in expression from group II to VI (Figure 7B). In addition, significant differences in the PI of tumor cells (Figure 7D) were detected in groups I to VI—the tumor tissue

expression was highest in group I and lowest in group VI. Comparatively, the cell assay based on TUNEL expression (Figure 7C) revealed the highest apoptosis in group VI compared with the other five groups ($P<0.05$). A remarkable AI variance (Figure 7E) was observed in the six groups, while the F3-PLGA@MB/Gd group showed the highest positive index with brown nuclear staining ($P<0.05$). These results indicated that the F3-PLGA@MB/Gd NPs combined with HIFU therapy can increase the efficiency of tumor ablation and induce tumor cell apoptosis in surrounding areas, thus killing residual tumor cells.

Regarding the mechanism of the HIFU synergistic effect caused by the introduction of F3-PLGA@MB/Gd NPs, two general factors are considered. First, the acoustic microenvironment could be changed due to the accumulation of NPs, thus leading to increased absorption of ultrasound waves and ultrasound energy deposition in the targeted tissue.[43] Due to the nanoscale particle sizes and the tumor-homing and penetrating peptides decorating the NP surface, the permeability of NPs in cancer tissues could be enhanced. Second, F3-PLGA@MB/Gd as a HIFU sonosensitizer experiences such high local temperatures that ROS are generated through pyrolysis reactions which can kill the remaining live tumor cells after HIFU ablation. Moreover, since ROS have very short half-lives,[44,45] the tumor cells could be more affected when F3-targeted NPs are incorporated. Taken together, the combination of HIFU ablation and simultaneous SDT by the introduction of F3-PLGA@MB/Gd as a sonosensitizer enhanced the ablation efficiency of HIFU and aided in killing the residual live cancer cells, thus leading inhibition of the tumor.

It should be noted that this study examined only short-term effects of SDT and HIFU multimodal therapy. For complete regression of tumors in vivo, further improvements of the F3-PLGA@MB/Gd and HIFU combined treatment are needed. Moreover, we only detected ROS in vitro, and thus, an evaluation of ROS during the HIFU irradiation experiment in vivo was lacking. We obtained indirect evidence of the ablation synergistic effect via the immunohistochemical assay, which will be further evaluated in subsequent experiments.

Notwithstanding these limitations, this study suggests that combination treatment of HIFU and SDT can enhance therapeutic outcomes. Thus, this treatment could be a key strategy to achieve a synergistic effect of killing tumor cells.

Conclusion

We describe a newly developed nanosized theranostic agent, F3-PLGA@MB/Gd, which was fabricated using F3-conjugated and MB/Gd-DTPA-BMA encapsulated PLGA NPs. The F3-PLGA@MB/Gd NPs exhibited excellent tumor-homing PA and MRI imaging properties that enhanced the sonodynamic effect and sonication-induced hyperthermia under HIFU irradiation. Furthermore, the synergistic SDT and HIFU therapy could overcome the limitations of single sonodynamic therapy or HIFU ablation and enhance the treatment efficiency. Our results indicate that the multifunctional F3-PLGA@MB/Gd nanocarriers together with the SDT and HIFU synergistic therapy could be used in new approaches for cancer therapy and have potential for further clinical applications.

Acknowledgments

Disclosure

The authors report no conflicts of interest in this work.

References

1. Peek MC, Ahmed M, Napoli A, Usiskin S, Baker R, Douek M. Minimally invasive ablative techniques in the treatment of breast cancer: a systematic review and meta-analysis. *Int J Hyperthermia*. 2017;33(2):191–202.
2. Zhou Y, Han X, Jing X, Chen Y. Construction of silica-based micro/nanoplatforms for ultrasound theranostic biomedicine. *Adv Healthc Mater*. 2017;6(18):1700646. doi:10.1002/adhm.201700646
3. Tachibana K. Emerging technologies in therapeutic ultrasound: thermal ablation to gene delivery. *Hum Cell*. 2004;17(1):7–15.
4. Chen H, Zhou X, Gao Y, Zheng B, Tang F, Huang J. Recent progress in development of new sonosensitizers for sonodynamic cancer therapy. *Drug Discov Today*. 2014;19(4):502–509. doi:10.1016/j.drudis.2014.01.010
5. Chen Y, Chen H, Shi J. Nanobiotechnology promotes noninvasive high-intensity focused ultrasound cancer surgery. *Adv Healthc Mater*. 2015;4(1):158–165. doi:10.1002/adhm.201400127

6. Hu CM, Zhang L. Nanoparticle-based combination therapy toward overcoming drug resistance in cancer. *Biochem Pharmacol*. 2012;83 (8):1104–1111. doi:10.1016/j.bcp.2012.01.008

7. Han H, Lee H, Kim K, Kim H. Effect of high intensity focused ultrasound (HIFU) in conjunction with a nanomedicines-microbubble complex for enhanced drug delivery. *J Controlled Release*. 2017;266:75–86. doi:10.1016/j.jconrel.2017.09.022

8. Hallez L, Touyeras F, Hihn JY, Bailly Y. Characterization of HIFU transducers designed for sonochemistry application: acoustic streaming. *Ultrason Sonochem*. 2016;29:420–427. doi:10.1016/j.ultsonch.2015.10.019

9. Hallez L, Touyeras F, Hihn JY, et al. Characterization of HIFU transducers designed for sonochemistry application: cavitation distribution and quantification. *Ultrasonics*. 2010;50(2):310–317. doi:10.1016/j.ultras.2009.09.011

10. Wang L, Niu M, Zheng C, et al. A core-shell nanoplatform for synergistic enhanced sonodynamic therapy of hypoxic tumor via cascaded strategy. *Adv Healthc Mater*. 2018;7(22):e1800819. doi:10.1002/adhm.201800819

11. Costley D, Mc Ewan C, Fowley C, et al. Treating cancer with sonodynamic therapy: a review. *Int J Hyperthermia*. 2015;31(2):107–117. doi:10.3109/02656736.2014.992484

12. Huang P, Qian X, Chen Y, et al. Metalloporphyrin-encapsulated biodegradable nanosystems for highly efficient magnetic resonance imaging-guided sonodynamic cancer therapy. *J Am Chem Soc*. 2017;139(3):1275–1284. doi:10.1021/jacs.6b11846

13. He Y, Wan J, Yang Y, et al. Multifunctional polypyrrole-coated mesoporous TiO2 nanocomposites for photothermal, sonodynamic, and chemotherapeutic treatments and dual-modal ultrasound/photoacoustic imaging of tumors. *Adv Healthc Mater*. 2019;8(9):e1801254. doi:10.1002/adhm.201801254

14. Suehiro S, Ohnishi T, Yamashita D, et al. Enhancement of antitumor activity by using 5-ALA-mediated sonodynamic therapy to induce apoptosis in malignant gliomas: significance of high-intensity focused ultrasound on 5-ALA-SDT in a mouse glioma model. *J Neurosurg*. 2018;129 (6):1416–1428. doi:10.3171/2017.6.JNS162398

15. Deepagan VG, You DG, Um W, et al. Long-circulating Au-TiO2 nanocomposite as a Sonosensitizer for ROS-mediated eradication of cancer. *Nano Lett*. 2016. doi:10.1021/acs.nanolett.6b02547

16. Qian X, Zheng Y, Chen Y. Micro/nanoparticle-augmented Sonodynamic Therapy (SDT): breaking the depth shallow of photoactivation. *Adv Mater*. 2016;28(37):8097–8129. doi:10.1002/adma.201602012

17. Sahu A, Choi WI, Lee JH, Tae G. Graphene oxide mediated delivery of methylene blue for combined photodynamic and photothermal therapy. *Biomaterials*. 2013;34(26):6239–6248. doi:10.1016/j.biomaterials.2013.04.066

18. Aoyama T, Fujikawa H, Cho H, et al. A methylene blue-assisted technique for harvesting lymph nodes after radical surgery for gastric cancer: a prospective, randomized, controlled study. *Am J Surg Pathol*. 2015;39(2):266–273. doi:10.1097/PAS.0000000000000336

19. Erpelding TN, Kim C, Pramanik M, et al. Sentinel lymph nodes in the rat: noninvasive photoacoustic and US imaging with a clinical US system. *Radiology*. 2010;256(1):102–110. doi:10.1148/radiol.10091772

20. He LL, Wang X, Wu XX, et al. Protein damage and reactive oxygen species generation induced by the synergistic effects of ultrasound and methylene blue. *Spectrochim Acta A Mol Biomol Spectrosc*. 2015;134:361–366. doi:10.1016/j.saa.2014.06.121

21. Xiang J, Leung AW, Xu C. Effect of ultrasound sonication on clonogenic survival and mitochondria of ovarian cancer cells in the presence of methylene blue. *J Ultrasound Med*. 2014;33(10):1755–1761. doi:10.7863/ultra.33.10.1755

22. Morgounova E, Shao Q, Hackel BJ, Thomas DD, Ashkenazi S. Photoacoustic lifetime contrast between methylene blue monomers and self-quenched dimers as a model for dual-labeled activatable probes. *J Biomed Opt*. 2013;18(5):56004. doi:10.1117/1.JBO.18.5.056004

23. Khdair A, Gerard B, Handa H, Mao G, Shekhar MP, Panyam J. Surfactant-polymer nanoparticles enhance the effectiveness of anticancer photodynamic therapy. *Mol Pharm*. 2008;5(5):795–807. doi:10.1021/mp800026t

24. Qin M, Hah HJ, Kim G, Nie G, Lee YE, Kopelman R. Methylene blue covalently loaded polyacrylamide nanoparticles for enhanced tumor-targeted photodynamic therapy. *Photochem Photobiol Sci*. 2011;10(5):832–841. doi:10.1039/c1pp05022b

25. Wu D, Gao Y, Qi Y, Chen L, Ma Y, Li Y. Peptide-based cancer therapy: opportunity and challenge. *Cancer Lett*. 2014;351(1):13–22. doi:10.1016/j.canlet.2014.05.002

26. Majumder P, Bhunia S, Bhattacharyya J, Chaudhuri A. Inhibiting tumor growth by targeting liposomally encapsulated CDC20siRNA to tumor vasculature: therapeutic RNA interference. *J Controlled Release*. 2014;180:100–108. doi:10.1016/j.jconrel.2014.02.012

27. Lin M-C, Lin S-B, Chen J-C, Hui C-F, Chen J-Y. Shrimp antilipopolysaccharide factor peptide enhances the antitumor activity of cisplatin in vitro and inhibits HeLa cells growth in nude mice. *Peptides*. 2010;31(6):1019–1025. doi:10.1016/j.peptides.2010.02.023

28. Feng X, Jiang D, Kang T, et al. Tumor-homing and penetrating peptide-functionalized photosensitizer-conjugated PEG-PLA nanoparticles for chemo-photodynamic combination therapy of drug-resistant cancer. *ACS Appl Mater Interfaces*. 2016;8(28):17817–17832. doi:10.1021/acsami.6b04442

29. Danhier F, Ansorena E, Silva JM, Coco R, Le Breton A, Preat V. PLGA-based nanoparticles: an overview of biomedical applications. *J Controlled Release*. 2012;161(2):505–522. doi:10.1016/j.jconrel.2012.01.043

30. Yu J, Nguyen HNY, Steenbergen W, Kim K. Recent development of technology and application of photoacoustic molecular imaging toward clinical translation. *J Nucl Med*. 2018. doi:10.2967/jnumed.117.201459

31. Haris M, Yadav SK, Rizwan A, et al. Molecular magnetic resonance imaging in cancer. *J Transl Med*. 2015;13:313. doi:10.1186/s12967-015-0541-x

32. Froehlich K, Haeger JD, Heger J, et al. Generation of multicellular breast cancer tumor spheroids: comparison of different protocols. *J Mammary Gland Biol Neoplasia*. 2016;21(3–4):89–98. doi:10.1007/s10911-016-9359-2

33. Aftab S, Shah A, Nadhman A, et al. Nanomedicine: an effective tool in cancer therapy. *Int J Pharm*. 2018;540(1–2):132–149. doi:10.1016/j.ijpharm.2018.02.007

34. Suk JS, Xu Q, Kim N, Hanes J, Ensign LM. PEGylation as a strategy for improving nanoparticle-based drug and gene delivery. *Adv Drug Deliv Rev*. 2016;99(Pt A):28–51. doi:10.1016/j.addr.2015.09.012

35. Moura V, Lacerda M, Figueiredo P, et al. Targeted and intracellular triggered delivery of therapeutics to cancer cells and the tumor microenvironment: impact on the treatment of breast cancer. *Breast Cancer Res Treat*. 2012;133(1):61–73. doi:10.1007/s10549-011-1688-7

36. Fonseca NA, Rodrigues AS, Rodrigues-Santos P, et al. Nucleolin overexpression in breast cancer cell sub-populations with different stem-like phenotype enables targeted intracellular delivery of synergistic drug combination. *Biomaterials*. 2015;69:76–88. doi:10.1016/j.biomaterials.2015.08.007

37. Hu Q, Gu G, Liu Z, et al. F3 peptide-functionalized PEG-PLA nanoparticles co-administrated with tLyp-1 peptide for anti-glioma drug delivery. *Biomaterials*. 2013;34(4):1135–1145. doi:10.1016/j.biomaterials.2012.10.048

38. Dai L, Yu Y, Luo Z, et al. Photosensitizer enhanced disassembly of amphiphilic micelle for ROS-response targeted tumor therapy in vivo. *Biomaterials*. 2016;104:1–17. doi:10.1016/j.biomaterials.2016.07.002

39. Pan X, Bai L, Wang H, et al. Metal-organic-framework-derived carbon nanostructure augmented sonodynamic cancer therapy. *Adv Mater*. 2018;30(23):e1800180. doi:10.1002/adma.201800180

40. Chen J, Luo H, Liu Y, et al. Oxygen-self-produced nanoplatform for relieving hypoxia and breaking resistance to sonodynamic treatment of pancreatic cancer. *ACS Nano*. 2017;11(12):12849–12862. doi:10.1021/acsnano.7b08225

41. Zhang X, Zheng Y, Wang Z, et al. Methotrexate-loaded PLGA nanobubbles for ultrasound imaging and synergistic targeted therapy of residual tumor during HIFU ablation. *Biomaterials*. 2014;35 (19):5148–5161. doi:10.1016/j.biomaterials.2014.02.036

42. Sun Y, Zheng Y, Ran H, et al. Superparamagnetic PLGA-iron oxide microcapsules for dual-modality US/MR imaging and high intensity focused US breast cancer ablation. *Biomaterials*. 2012;33(24):5854–5864. doi:10.1016/j.biomaterials.2012.04.062

43. You Y, Wang Z, Ran H, et al. Nanoparticle-enhanced synergistic HIFU ablation and transarterial chemoembolization for efficient cancer therapy. *Nanoscale*. 2016;8(7):4324–4339. doi:10.1039/c5nr08292g

44. Hatz S, Lambert JD, Ogilby PR. Measuring the lifetime of singlet oxygen in a single cell: addressing the issue of cell viability. *Photochem Photobiol Sci*. 2007;6(10):1106–1116. doi:10.1039/b707313e

45. Zhang D, Wen L, Huang R, Wang H, Hu X, Xing D. Mitochondrial specific photodynamic therapy by rare-earth nanoparticles mediated near-infrared graphene quantum dots. *Biomaterials*. 2018;153:14–26. doi:10.1016/j.biomaterials.2017.10.034

Supplementary materials
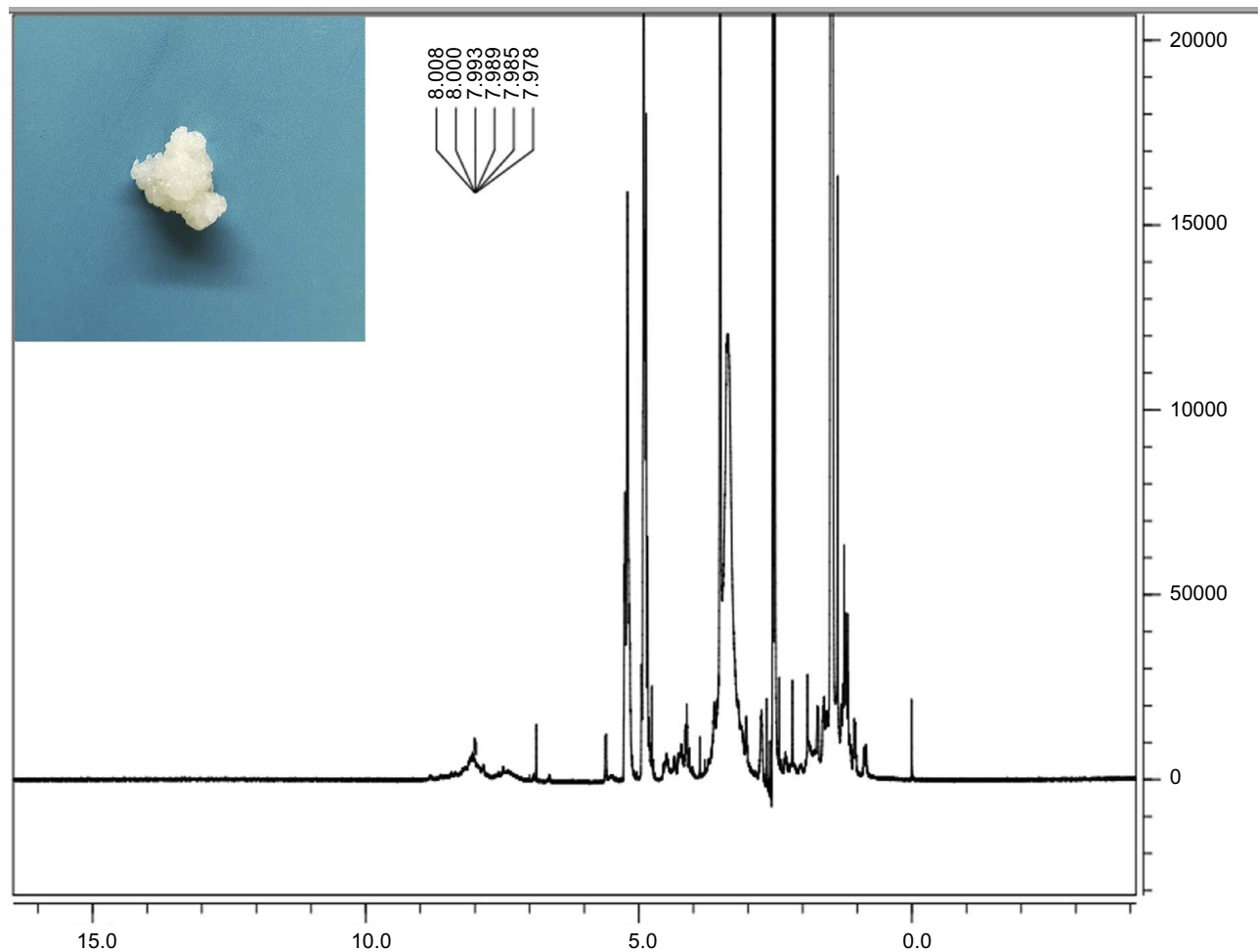
Figure S1 Digital photo of MAL-PEG-PLGA-F3 and ^{1}H NMR spectra of MAL-PEG-PLGA-F3 (7.0–8.0 F3 peptide, 3.5 PEG, 3.3 MAL, 4.5–5.5 and 1.0–1.5 PLGA).
Abbreviations: MAL, maleimide; PEG, polyethylene glycol; PLGA, poly(lactide-co-glycolic acid); NMR, nuclear magnetic resonance.
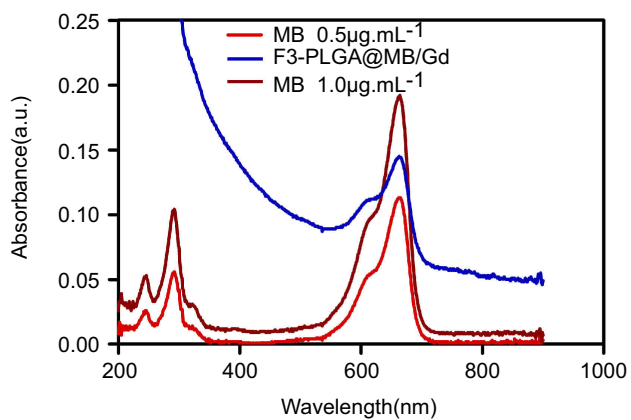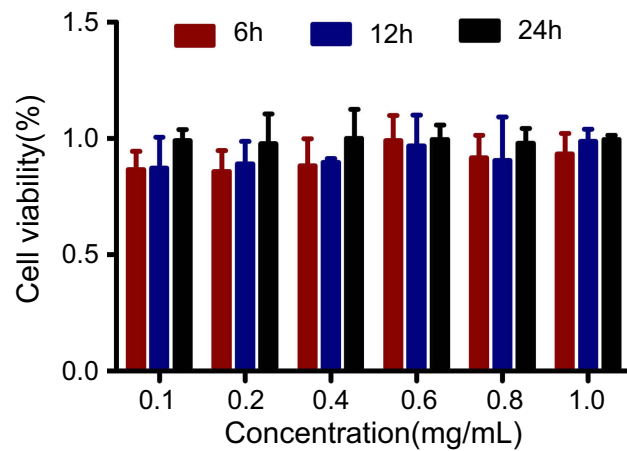

Figure S2 UV-visible spectrum of free MB and F3-PLGA@MB/Gd nanoparticles.
Abbreviations: UV, ultraviolet spectrum; MB, methylene blue; PLGA, poly(lactide-co-glycolic acid); Gd, gadodiamide.
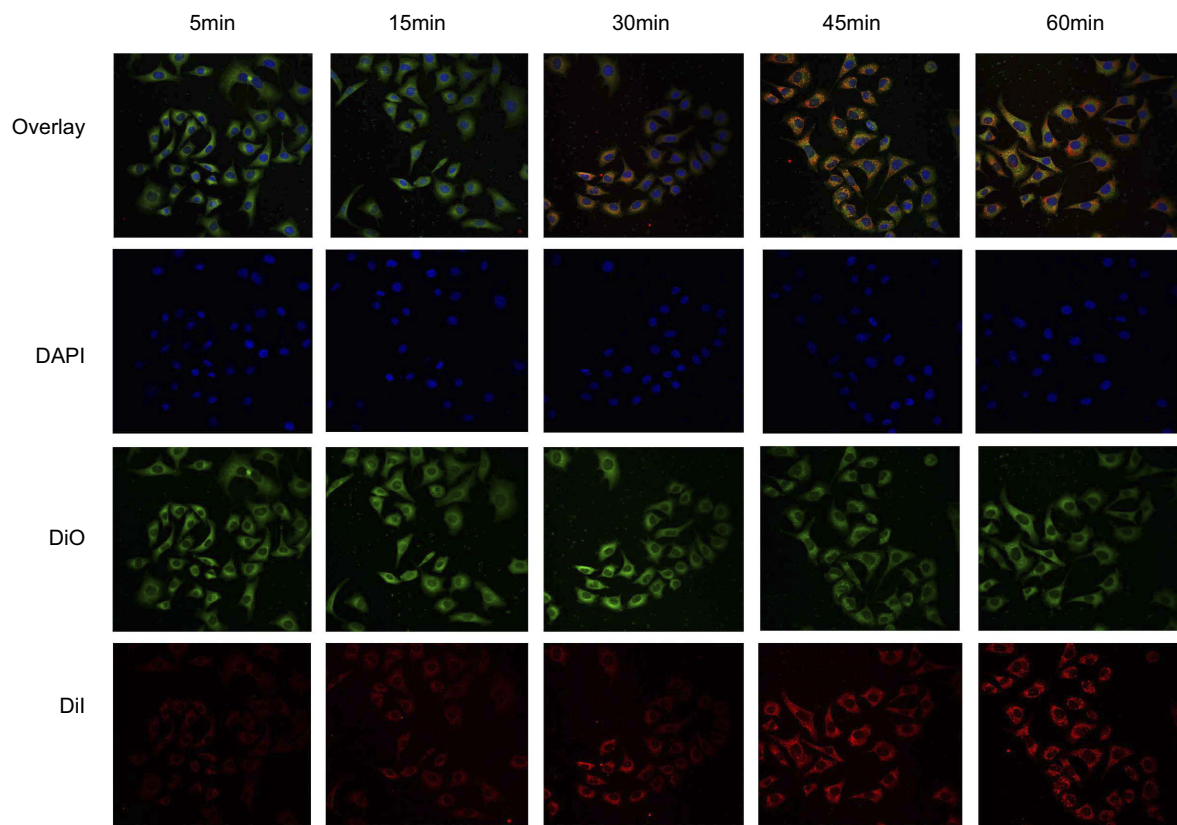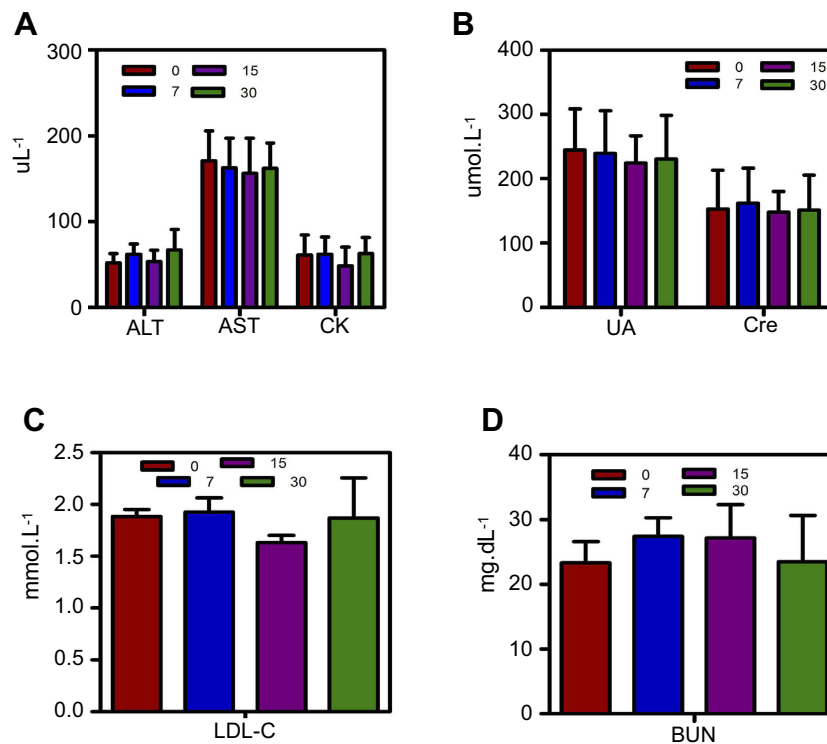
Figure S3 Cellular uptake of nanoparticles within one hour. Scale bar: 50 μm.
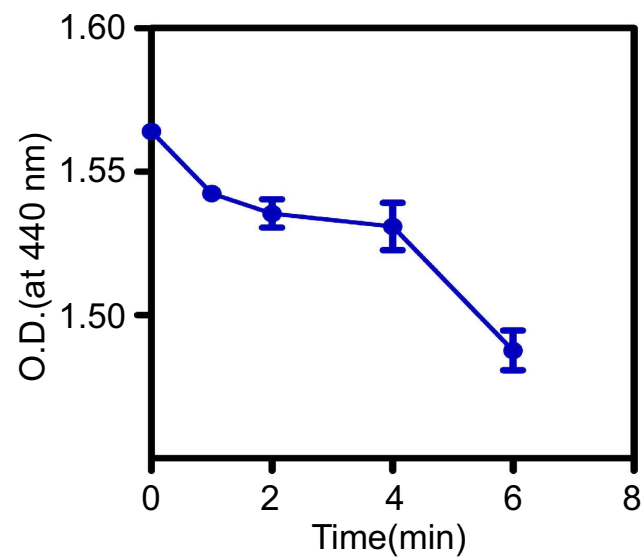
Figure S4 $^1O_2$ generation by F3-PLGA@MB/Gd NPs after US irradiation for different time periods.

Figure S5 Cytotoxicity against MB-231 cells with F3-PLGA@MB/Gd.
Abbreviations: PLGA, poly(lactide-co-glycolic acid); MB, methynele blue; Gd, gadodiamide.

Figure S6 Liver function (ALT, AST), renal function (BUN, UA, Cre), and heart function (CK, LDL-C) of mice before injection and at 7-day, 14-day, 30-day after intravenous injection of F3-PLGA@MB/Gd.